Journal of Molecular Spectroscopy 254 (2009) 78–86

Contents lists available at ScienceDirect

Journal of Molecular Spectroscopy

journal homepage: www.elsevier.com/locate/jms

The rotational spectrum of chlorine nitrate ($ClONO_2$) in the four lowest nv_9 polyads

Zbigniew Kisiel [a,*], Ewa Białkowska Jaworska [a], Rebecca A.H. Butler [b], Douglas T. Petkie [c], Paul Helminger [d], Ivan R. Medvedev [e], Frank C. De Lucia [e]

[a] Institute of Physics, Polish Academy of Sciences, Al. Lotników 32/46, PL-02-668 Warszawa, Poland
[b] Department of Physics, Pittsburg State University, Pittsburg, KS 66762, USA
[c] Department of Physics, Wright State University, Dayton, OH 45435, USA
[d] Department of Physics, University of South Alabama, Mobile, AL 36688, USA
[e] Department of Physics, The Ohio State University, Columbus, OH 43210-1106, USA

ARTICLE INFO

Article history:
Received 3 December 2008
In revised form 6 January 2009
Available online 24 January 2009

Keywords:
Chlorine nitrate
$ClONO_2$
Millimeter wave rotational spectrum
Excited vibrational states
Interstate interactions
Coriolis coupling
Fermi resonance
Remote sensing
Atmosphere

ABSTRACT

The analysis of the recently recorded 78–378 GHz broadband spectrum of $ClONO_2$ has been extended to cover rotational transitions in all 14 excited vibrational states up to 650 cm^{-1} above the ground state. We report new measurements and analysis of the $2v_9$ and $3v_9$ dyads, and first assignment and analysis for the $4v_9$ and $5v_9$ triads. The polyad fits encompass a total of over 20000 newly measured transition frequencies and spectroscopic constants are reported for 10 vibrationally excited states in each of $^{35}ClONO_2$ and $^{37}ClONO_2$. All polyads were fitted with a new coupling scheme between the perturbing states combining *c*-axis Coriolis and Fermi interactions. The scheme is validated by multiple tests of the physical significance of the derived parameters and it results in improved deviations of fits and significant reduction in the number of adjustable parameters.

© 2009 Elsevier Inc. All rights reserved.

1. Introduction

Chlorine nitrate, $ClONO_2$, is a molecule of considerable environmental importance since it is a participant in the atmospheric chlorine cycle [1]. Rotational structures of the chlorine nitrate infrared bands have been difficult to establish due to spectral overlap even in the Doppler limit, so that remote sensing recoveries are based on band spectra approaches rather than line-by-line calculations [2–4]. Nevertheless, reports of analyses of the rotation-vibration spectra are beginning to appear. These include the spectra of cooled molecular beams [1,5], but the low temperature of these beams does not populate states that are important in the spectra at atmospheric temperatures. Analyses of resolved lines and band contours have already been used to provide the basis for simulations and atmospheric retrievals [6].

One of the motivations for the work reported here is to use the higher resolution in the millimeter/submillimeter (mm/submm) region to resolve this otherwise difficult to observe rotational structure and to develop quantum mechanical spectroscopic models. We have shown in the case of the spectrally complex $v_5/2v_9$ dyad of HNO_3 [7] that the knowledge of the rotational structure of the relevant excited states obtained from the mm/submm spectrum is sufficient to calculate its vibration-rotation energy level structure to very high accuracy. We have also used this approach to simulate the rotational structure of the infrared bands of HNO_3 in the 22 μ region [8]. It is our goal to be able to synthesize on a line-by-line basis (including hot bands and isotopologues) the rotational structure of as many infrared bands of $ClONO_2$ as possible. Based on this work and work on the states for which we have at least preliminary analyses [9], we expect that these simulations will be possible through at least $v_4 = 1$ at ≈780 cm^{-1} without the use of deconvolution techniques.

However, this mm/submm approach faces its own challenges, especially for $ClONO_2$. First, the pure rotational spectra in excited vibrational states are effectively hot bands and their intensities are reduced by their corresponding Boltzmann factor. This is, however, not the most fundamental challenge since the sensitivity of modern mm/submm spectroscopy is such that for similar molecules even high lying levels are of sufficient intensity to be observed. For example, we have measured and analyzed the v_2 state of HNO_3 near 1700 cm^{-1} with integration times of ≈10^{-3} s. The more fundamental challenge is the aforementioned spectral congestion that results from all of the many hot bands sharing the same spectral space in the rotational spectrum, and the additional crowding introduced by the presence of two abundant chlorine isotopes.

* Corresponding author. Fax: +48 22 8430926.
E-mail address: kisiel@ifpan.edu.pl (Z. Kisiel).

0022-2852/$ - see front matter © 2009 Elsevier Inc. All rights reserved.
doi:10.1016/j.jms.2009.01.005

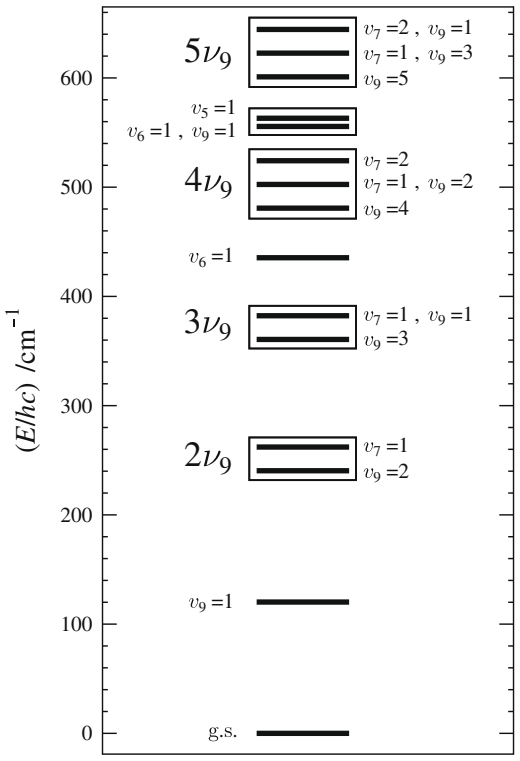

Fig. 1. Positions of lowest vibrational energy states in $^{35}ClONO_2$. Rectangles enclose polyads of interacting states treated by means of coupled state fits. Dark lines indicate states investigated in this work, and the polyads are labelled according to their lowest constituent state. The remaining states have most recently been studied in [16,17].

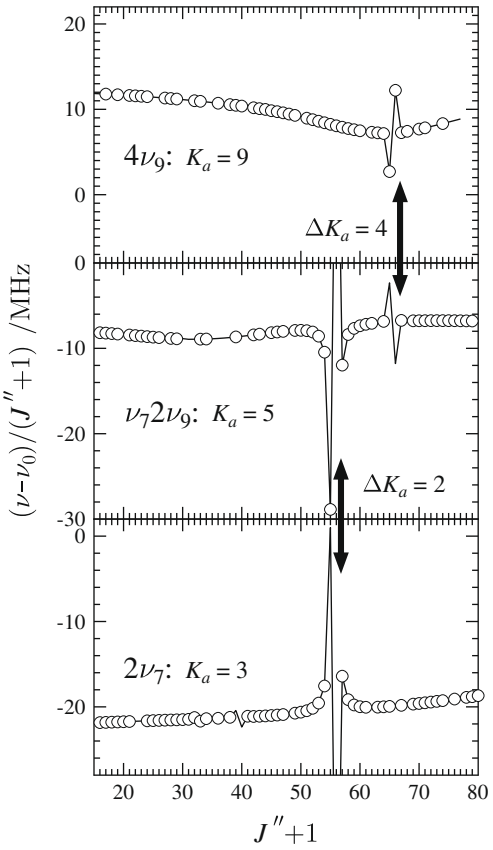

Fig. 2. Illustration of some of the many possible level-crossing type perturbations taking place between rotational levels in the $4v_9$ triad in $^{35}ClONO_2$. The plot is of the difference between the frequency of a given excited state transition and its counterpart in the ground state. The differences are scaled by $J + 1$, the circles mark assigned lines and the continuous lines are for frequencies calculated from the final fit. The plotted sequences are all for ^{a}R-type transitions between rotational levels with $K_a + K_c = J + 1$.

The pure rotation spectrum of chlorine nitrate has been investigated on many previous occasions [10–17]. The chlorine nitrate molecule has several low frequency vibrational modes such that, even for moderate vibrational energies of up to 650 cm^{-1}, there are already 14 different excited vibrational states, see Fig. 1. The number of states is effectively doubled if the ^{37}Cl isotopologue is taken into account, giving rise to a correspondingly rich room-temperature rotational spectrum. The most precise currently available constants have been obtained from the analysis of a new broadband rotational spectrum of chlorine nitrate recorded with synthesizer and FASSST spectroscopic techniques, and are for the ground state and four of the excited states [16,17]. The remaining 10 excited vibrational states up to 650 cm^{-1} are grouped into four polyads of strongly interacting states as a consequence of a near 1:2 ratio in the frequencies of the v_9 and v_7 normal modes. The two lowest polyads, the $2v_9$ dyad and the $3v_9$ dyad, have already been analysed in older spectra, [13,14]. Nevertheless, even though the measured transition frequencies were satisfactorily reproduced, it was realised that the derived spectroscopic constants were more effective than physical [15]. We have presently reinvestigated the construction of the Hamiltonian in order to be able to fit the interactions in all four lowest nv_9 polyads in a unified manner. The most recent spectra were used to reinvestigate the two dyads, and also to assign and fit transitions in the $4v_9$ and $5v_9$ triads.

2. Experimental details

Analysis was carried out on the same broadband rotational spectrum that was used in the immediately preceding work [16,17]. This single spectrum consists of two joined segments, a 78–118 GHz section recorded with a KVARTZ mm-wave synthesizer [9], and a 118–378 section recorded with the FASSST (FAst Scan Submillimeter Spectrometer Technique) spectrometer [18–20]. Analysis of the spectrum up to the level of the $5v_9$ triad required keeping track of lines assigned in 30 different vibrational states, 15 each for $^{35}ClONO_2$ and $^{37}ClONO_2$. This was carried out by means of the AABS package for Assignment and Analysis of Broadband Spectra [21,22], which was also used to construct the data sets. Various graphical techniques for assigning lines and following the interstate perturbations have been employed, as described in detail in the analysis of the FASSST spectrum of the $S(CN)_2$ molecule [23]. Pickett's SPFIT/SPCAT program package [24,25] was used for fitting and prediction.

3. Rotational spectrum

$ClONO_2$ is a planar molecule and its rotational spectrum is dominated by ^{a}*R*-type transitions since the $\mu_a = 0.72(7)$D dominates over the other non-zero component $\mu_b = 0.24(2)$D [10]. Weak ^{b}*Q*-type transitions are only assignable in the lower vibrational states. Rotational transitions in the polyads are subject to multiple perturbations, as has already been shown for the $2v_9$ dyad in [13]. A sample of the perturbations occurring between the states in the newly studied $4v_9$ triad is illustrated in Fig. 2 by means of a simple scaled frequency difference plot. It can be seen that transitions in the single $K_a = 5$ line sequence in the central $v_7 2v_9$ state are perturbed by $\Delta K_a = 4$ interactions with the lower $4v_9$ state and by $\Delta K_a = 2$ interactions with the upper $2v_7$ state. This is demonstrated by the mirror image appearance of the plots, which were constructed relatively easily by using the graphical Loomis–Wood type assignment techniques built into the AABS package [21,23]. The more

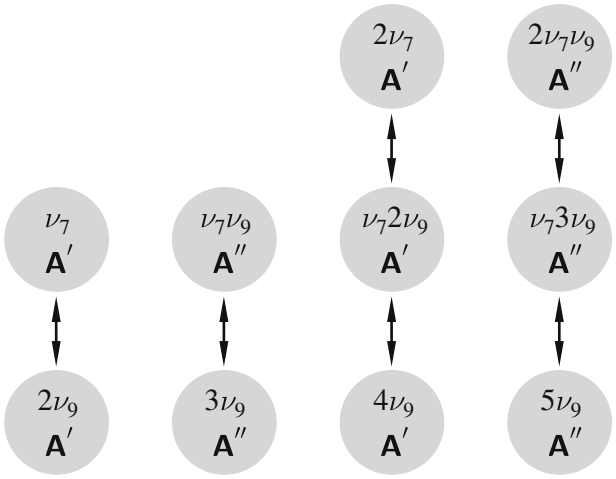

Fig. 3. Summary of the interstate interactions accounted for in analysis of the $n\nu_9$ polyads. The states in each polyad are of the same symmetry so that each pair of states can be connected by *c*-axis Coriolis and Fermi resonance terms. The outer states in the two triads turn out to be sufficiently separated so that no corresponding connecting terms are necessary. All interactions are of the type $(v_7-1,v_9+2)\Leftrightarrow(v_7,v_9)$, with $v_7=1$ for the lower pairs of states, and $v_7=2$ for the upper pairs.

perturbed lines could only be assigned at an advanced stage of the fitting procedure. The need to fit multiple instances of such behaviour in the $4\nu_9$ and $5\nu_9$ triads posed a considerable challenge, while we found it difficult to build on the otherwise successful fits reported for the $2\nu_9$ and $3\nu_9$ dyads [13,14] since those used somewhat different forms of the Hamiltonian. The realisation of the effective nature of the previous results [15] and the expectation that a more unified construction of the Hamiltonian for the strongly related $n\nu_9$ polyads should be possible prompted us to reinvestigate the construction of the Hamiltonian used to in the fits.

3.1. The Hamiltonian

The symmetries of states comprising the $n\nu_9$ polyads are summarised in Fig. 3 and it can be seen that all states in a given polyad are of the same symmetry. For even values of *n* all states in a polyad belong to the *A*′ irreducible representation of the C_s point group of the molecule, while for odd *n* all states belong to the *A*″ representation. The direct products $A'\otimes A'$ and $A''\otimes A''$ are both equal to *A*′, which contains the rotation species R_c. Thus, according to Jahn's rule [26], each pair of states in a polyad can, in principle, interact by means of the Coriolis coupling mechanism around the *c*-rotational axis. Furthermore, since all states in a polyad are of the same symmetry, they can also perturb by means of the Fermi resonance. The Hamiltonian for each polyad will be in block form with respect to the vibrational identifiers for the interacting states. We employed the following 2×2 Hamiltonian for the dyads

$$\begin{pmatrix} H_r^{(v)} & H_{\rm cor}^{(v,v')}+H_F^{(v,v')} \\ H_{\rm cor}^{(v,v')}+H_F^{(v,v')} & H_r^{(v')}+\Delta E_0^{(v,v')} \end{pmatrix} \quad (1)$$

and the simplified 3×3 Hamiltonian for the triads

$$\begin{pmatrix} H_r^{(v)}-\Delta E_0^{(v,v')} & H_{\rm cor}^{(v,v')}+H_F^{(v,v')} & 0 \\ H_{\rm cor}^{(v,v')}+H_F^{(v,v')} & H_r^{(v')} & H_{\rm cor}^{(v',v'')}+H_F^{(v',v'')} \\ 0 & H_{\rm cor}^{(v',v'')}+H_F^{(v',v'')} & H_r^{(v'')}+\Delta E_0^{(v',v'')} \end{pmatrix}. \quad (2)$$

The diagonal blocks consist of the rotational Hamiltonian for the pertinent states, $H_r^{(v)}$ etc., augmented by the appropriate energy level separation $\Delta E_0^{(v,v')}=E_{v'}-E_v$ etc. between vibrationally unperturbed levels. For the triads it was convenient to define the energy separations relative to the energy of the central state, which was set to zero. The H_r terms were set up using Watson's *S*-reduced asymmetric rotor Hamiltonian in representation I^r [27], since previous work on the rotational spectrum of $ClONO_2$ showed that *S*-reduction performed slightly better than the *A*-reduction.

The off-diagonal blocks in Eq. (1) and (2) are the sum of Coriolis and Fermi terms. For the triads it was found that it was not necessary to account for the interaction between the outer states so that the appropriate terms were set to zero. The leading terms for the Coriolis interaction result from the H_{21} and H_{22} parts of the vibration–rotation Hamiltonian [28], and are

$$H_{\rm cor}^{(v,v')}=i(G_c+G_c^J P^2+G_c^K P_z^2+\cdots)P_y+(F_{ab}+\cdots)(P_zP_x+P_xP_z). \quad (3)$$

In the present case the differences between vibrational indices of the interacting states exceed the condition for appreciable Coriolis coupling by the usual H_{21} term, which is that two vibrational quantum numbers should not differ by more than unity. All Coriolis interactions in the polyads will thus be of the higher order type arising from the H_{31} term in the vibration-rotation Hamiltonian. An

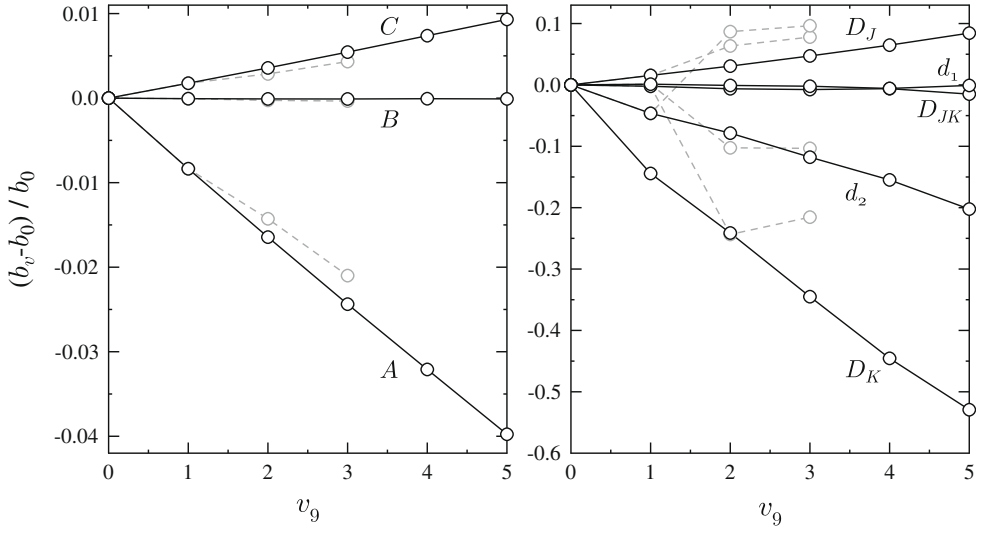

Fig. 4. Plots of scaled changes in selected fitted parameters for the $n\nu_9$ states: rotational constants (left) and quartic centrifugal distortion constants (right). Good consistency is visible between the results from current polyad fits and those for the isolated $v_9=1$ state (continuous lines). Dashed lines indicate results from previous fitting schemes used for the $2\nu_9$ and the $3\nu_9$ polyads, Refs.[13,14].

identical situation has originally been investigated in detail for the $(v_2+2,v_3-1)\Leftrightarrow(v_2,v_3)$ interactions in NO_2 [29]. It turns out that even though the leading Coriolis interaction constant, G_c, normally reflects the magnitude of the first order, H_{21} interaction, it also carries contributions from the third-rank H_{31} term in the vibration–rotation Hamiltonian [29,30]. In fact for the $2v_3\Leftrightarrow v_2$ interaction in NOBr the experimentally determined value of G_c was found to be precisely calculable from the H_{31} contribution [30]. Thus G_c and its centrifugal series are also expected to be the leading Coriolis interaction constants for the nv_9 polyads in $ClONO_2$.

The second contribution off-diagonal in v comes from the Fermi resonance and is of the form

$$H_F^{(v,v')} = W_F + W_F^J P^2 + W_F^K P_z^2 + W_F^{JJ} P^4 + W_F^{JK} P^2 P_z^2 + \cdots. \quad (4)$$

The Fermi term W_F has a direct effect on the energy level spacing between the interacting levels so that the actual (effective) energy level differences, ΔE, in the dyads and the triads resulting from the resonance are given by differences between the eigenvalues of

$$\begin{pmatrix} 0 & W_F^{(v,v')} \\ W_F^{(v,v')} & \Delta E_0^{(v,v')} \end{pmatrix} \quad \text{and} \quad \begin{pmatrix} -\Delta E_0^{(v,v')} & W_F^{(v,v')} & 0 \\ W_F^{(v,v')} & 0 & W_F^{(v',v'')} \\ 0 & W_F^{(v',v'')} & \Delta E_0^{(v',v'')} \end{pmatrix}, \quad (5)$$

respectively. The common practical difficulty encountered in analyses carried out using $H_{cor}^{(v,v')}$ in Eq. (3) to describe the Coriolis interactions is considerable correlation between G_c, F_{ab}, and the related rotational constant C corresponding to rotation about the coupling axis. In the present case it was not necessary to use F_{ab} but there were practically unitary intercorrelations between the values of ΔE_0 and W_F when fitting the Fermi interactions. However, the actual values of ΔE derived from Eq. (5) were very stable. Reliable estimates of their uncertainties required accounting for the intercorrelations by means of error propagation utilising also the off-diagonal elements of the variance–covariance matrix for the fit. In general, the estimated error σ_f on a derived quantity f, which is a function of n fitted parameters b_i, is given by

$$\sigma_f^2 = \sum_i \left(\frac{\partial f}{\partial b_i}\right)^2 \sigma_{b_i}^2 + 2\sum_i \sum_{j<i} \left(\frac{\partial f}{\partial b_i}\right)\left(\frac{\partial f}{\partial b_j}\right) c_{b_i,b_j}\sigma_{b_i}\sigma_{b_j}, \quad (6)$$

where σ_{b_i} is the error in a given parameter of fit and c_{b_i,b_j} is the correlation coefficient connecting two fitted parameters. Only the first term of Eq. (6) is normally used but the second term is critical when significant intercorrelations are present. The calculations were carried out numerically, although the analytical form of the 2×2 case provided a useful double check.

3.2. Results

The final results of the analysis of rotational transitions in the four lowest nv_9 polyads in both $^{35}ClONO_2$ and $^{37}ClONO_2$ are summarised in Tables 1–4. The primary data, comprising in each case of the results of fit file and of the source files for the SPFIT program, are reported in Tables S1–S8 of the Electronic Supplementary Information. All transitions were for simplicity equally weighted in the fits so that the resulting deviations of fit can also be used to assess the performance of the FASSST spectrometer. The achieved deviations are consistent with experience from the two immediately preceding studies of $ClONO_2$ [16,17] and that of $S(CN)_2$ [23], which benchmarked the frequency accuracy of the current version of the FASSST spectrometer at below 50 kHz. This deviation level has been achieved for the $2v_9$ dyad and the deviations of fit show a similar increase with vibrational energy to that seen for $S(CN)_2$ in which there is a similar dense structure of low lying vibrational energy levels.

The results for the $2v_9$ dyad are particularly instructive. The dataset for this dyad has been appreciably extended in precision and in the number of measured transitions. In our previous study 3180 transitions for $^{35}ClONO_2$ were fitted to within 113.5 kHz, while presently we fit 3800 transition frequencies to 45.3 kHz. We have now used only 23 adjustable parameters to compare with 42 parameters used previously [13]. Interestingly the new dataset, which contains many strongly perturbed transitions and some interstate transitions, is still satisfactorily enough fitted with the old scheme, at a respectable deviation of fit of 61.4 kHz. The results of the two alternative fits of the new data are compared in more detail in Table S9, and one possible pragmatic conclusion is that the available data are almost equally well described by both schemes. The advance is mainly in the economy of fit and in the physical meaning of the derived parameters.

The current fits for all polyads did not require fitting any of the sextic centrifugal distortion parameters as it was sufficient to fix their values at those from the ground state. The fitted values of all rotational constants are now much closer to harmonic behaviour as demonstrated for the v_9 series of states in the left-hand plot in Fig. 4. The values for all of the perturbed $v_9 > 1$ states are seen to be a good linear extrapolation of the change between the ground state and the unperturbed $v_9 = 1$. The right pane of Fig. 4 shows that a similar situation is the case for the quartic centrifugal distortion constants. A single number that provides a check of the deperturbed nature of the fitted rotational constants is the inertial defect, $\Delta_i = I_c - I_a - I_b$. The values of this quantity for a planar molecule are well calculable from the harmonic force field and are a particularly useful benchmark for states, such as $v_7 = 1$, for which unperturbed rotational constants are not directly available. The current experimental values of inertial defects for all states in the four nv_9 polyads are compared in Table 5 with values calculated in Ref. [12] from the fitted harmonic force field for $ClONO_2$. The agreement is seen to be excellent while effective solutions such as those obtained previously have a tendency to produce symmetrically opposed exp.–calc. deviations. This is an invaluable indicator for guiding the perturbation fits, which are notorious for getting stuck in local minima and need considerable perseverance in order to locate the global minimum.

The final tool used in reaching the reported fits are the distribution plots of mixing coefficients and obs.–calc. values, as successfully applied previously for the $v_5\Leftrightarrow v_6v_9$ dyad in $ClONO_2$ [16] and the polyads in $S(CN)_2$ [23]. Plots of this type for the $4v_9$ triad in $^{35}ClONO_2$ are reproduced in Fig. 5. The left-hand plot is based of the mixing coefficients, P_{mix} that are listed in SPCAT output. The values of $1 - P_{mix}$ give a direct indication of how much a given energy level is perturbed or mixes with levels from different vibrational states. In this way it is possible to obtain an automatically generated overview of the perturbations in the complete data set. There is one difference relative to the plots used earlier in that presently there is a considerable but slowly changing contribution to the values of $1 - P_{mix}$ from the Fermi interaction, This considerably complicates the appearance of such plot so that such contribution was filtered out for clarity. The perturbations between different vibrational states can be easily matched since a given pairwise perturbation is expected to take place for the same value of J and will be at higher K_a for the lower vibrational level. Once this is done it is possible to transfer the identified perturbation regions to an overview of the actual data set in the form of the right-hand plots in Fig. 5 of magnitudes of obs.–calc. values for the measured lines. Analysis of the spectrum can then be tailored towards adding to the data of transitions that carry more information about the interactions. In this way it is easy to identify and then to explore in detail key regions such as the prominent $K_a = 13$ and $K_a = 11$ interaction between the two upper vibrational states in the triad. The resulting data is shown in the form of the more stan-

Table 1
Spectroscopic constants determined for the $2\nu_9$ dyad in $ClONO_2$, compared with those for the isolated ν_9 state.

	$^{35}ClONO_2$			$^{37}ClONO_2$		
	ν_9[a]	$2\nu_9$	ν_7	ν_9[a]	$2\nu_9$	ν_7
A (MHz)	12004.64061(28)[b]	11906.720(25)	12143.309(23)	12003.62660(49)	11905.184(52)	12142.675(52)
B (MHz)	2776.814605(50)	2776.7359(12)	2770.7929(11)	2700.868302(46)	2700.8658(22)	2694.9165(22)
C (MHz)	2262.133094(45)	2266.22014(35)	2250.34576(35)	2211.468529(45)	2215.43518(84)	2200.02545(88)
D_J (kHz)	0.508498(11)	0.516077(20)	0.499975(20)	0.488293(10)	0.495486(47)	0.480301(46)
D_{JK} (kHz)	3.845749(92)	3.83003(22)	3.92230(23)	3.70850(11)	3.69407(74)	3.77850(77)
D_K (kHz)	8.10675(62)	7.188(19)	10.683(20)	8.2395(25)	7.604(41)	10.201(45)
d_1 (kHz)	−0.0958169(67)	−0.0956221(72)	−0.0964201(72)	−0.0897908(89)	−0.089538(17)	−0.090337(17)
d_2 (kHz)	−0.0169201(31)	−0.0163485(60)	−0.0188995(69)	−0.0154106(18)	−0.014955(14)	−0.017215(14)
ΔE_0[c] (MHz)		411734.(89)			355525.(170)	
$\sigma_1 G_c$[d] (MHz)		335.977(21)			313.597(61)	
$\sigma_1 G_c^J$ (MHz)		−0.0006434(26)			−0.0007075(92)	
$\sigma_1 G_c^K$ (MHz)		−0.004261(59)			−0.00039(19)	
$\sigma_2 W_F$[d] (MHz)		145168.(63)			143124.(105)	
$\sigma_2 W_F^J$ (MHz)		−0.1138(25)			−0.1222(43)	
$\sigma_2 W_F^K$ (MHz)		−8.0684(69)			−7.394(13)	
σ_{fit} (MHz)	0.0479	0.0453[e]		0.0425	0.0498[e]	
N_{lines}	2523	3800		2006	2287	

[a] Ref. [17].
[b] Quantities in round parentheses are standard errors in units of the least significant digit of the constant.
[c] Energy difference between vibrationally unperturbed levels, $E(\nu_7) - E(2\nu_9)$.
[d] Only the relative signs of the various Coriolis and Fermi constants can be determined, so that σ_1 and σ_2 can independently be equal to +1 or −1.
[e] Sextic centrifugal distortion constants for the interacting states were fixed at values for the respective ground state, Ref. [16].

Table 2
Spectroscopic constants determined for the $3\nu_9$ dyad in $ClONO_2$.

	$^{35}ClONO_2$		$^{37}ClONO_2$	
	$3\nu_9$	$\nu_7\nu_9$	$3\nu_9$	$\nu_7\nu_9$
A (MHz)	11810.723(53)	12039.192(53)	11807.98(10)	12038.76(10)
B (MHz)	2776.7183(27)	2770.5299(26)	2700.8966(45)	2694.7644(45)
C (MHz)	2270.4418(13)	2254.3326(13)	2219.5185(21)	2203.9031(21)
D_J (kHz)	0.524373(55)	0.507897(54)	0.503241(88)	0.487586(88)
D_{JK} (kHz)	3.82503(71)	3.90328(72)	3.6941(15)	3.7519(16)
D_K (kHz)	6.205(29)	8.895(34)	5.910(50)	9.220(62)
d_1 (kHz)	−0.095497(17)	−0.096620(17)	−0.089670(31)	−0.090217(32)
d_2 (kHz)	−0.015653(10)	−0.017847(10)	−0.014144(24)	−0.016346(27)
ΔE_0[a] (MHz)	530286.(213)		469981.(359)	
$\sigma_1 G_c$[b] (MHz)	596.08(33)		558.40(84)	
$\sigma_1 G_c^J$ (MHz)	−0.001274(20)		−0.000918(27)	
$\sigma_1 G_c^K$ (MHz)	−0.00727(33)		−0.0099(10)	
$\sigma_2 W_F$[b] (MHz)	250594.(112)		247767.(170)	
$\sigma_2 W_F^J$ (MHz)	−0.2245(38)		−0.2586(61)	
$\sigma_2 W_F^K$ (MHz)	−13.9592(94)		−13.205(19)	
σ_{fit} (MHz)	0.0530[c]		0.0574[c]	
N_{lines}	3069		2055	

[a] Energy difference between vibrationally unperturbed levels, $E(\nu_7\nu_9) - E(3\nu_9)$.
[b] Only the relative signs of the various Coriolis and Fermi constants can be determined, so that σ_1 and σ_2 can independently be equal to +1 or −1.
[c] Sextic centrifugal distortion constants for the interacting states were fixed at values for the respective ground state, Ref. [16].

dard frequency difference plot in Fig. 6. The lack of any correlation between the magnitudes of obs.–calc. differences in Fig. 5 with the coloured areas transferred from the $(1 - P_{mix})$ plot demonstrates that the perturbations have been fitted successfully.

4. Discussion

The present work completes the assignment and analysis of the rotational spectrum of the $ClONO_2$ molecule for transitions in all vibrational states up to 650 cm^{-1} in vibrational energy. There are 14 excited vibrational states in this energy region, 10 of which belong to the four polyads analysed in this work. Improvements in the construction of the Hamiltonian used in fitting the polyads allowed all four polyads to be fitted in a unified way. The values of the key perturbation parameters for similar states in the polyads show practically linear evolution as illustrated for the main sequence of interacting levels in Fig. 7. However, even though the unperturbed energy differences, ΔE_0, change smoothly in the series there is a kink in the effective separation ΔE at the switch from the dyads to the triads, taking place between $3\nu_9$ and $4\nu_9$. This reflects the addition of one more vibrational level at higher energy in the triads, which would be expected to lead to a small compression in the energy level spacing of the lower doublet, as is indeed seen to be the case. The minor constants in the G_c and the W_F centrifugal series do not show the level of linearity visible in Fig. 7 for the major constants and probably mop up small effects that are outside the current fitting model. Thus the use of a global, Dunham type, fit for encompassing all polyads is deemed premature, since all the remaining vibrational states in the same energy region would probably also have to be added.

Table 3
Spectroscopic constants determined for the $4\nu_9$ triad in $ClONO_2$.

	$^{35}ClONO_2$			$^{37}ClONO_2$		
	$4\nu_9$	$\nu_7 2\nu_9$	$2\nu_7$	$4\nu_9$	$\nu_7 2\nu_9$	$2\nu_7$
A (MHz)	11717.24(12)	11937.736(96)	12181.448(36)	11714.30(25)	11936.26(19)	12181.124(68)
B (MHz)	2776.8063(65)	2770.3381(52)	2764.7157(16)	2701.050(13)	2694.653(11)	2688.9898(25)
C (MHz)	2274.8264(43)	2258.3858(41)	2242.62229(75)	2223.7587(65)	2207.8475(62)	2192.5209(14)
D_J (kHz)	0.533196(87)	0.515497(76)	0.499164(40)	0.51181(18)	0.49489(16)	0.479293(72)
D_{JK} (kHz)	3.8310(21)	3.8931(22)	3.97648(66)	3.7026(34)	3.7487(38)	3.8196(14)
D_K (kHz)	5.261(45)	7.516(46)	12.652(39)	5.37(14)	7.43(12)	13.087(87)
d_1 (kHz)	−0.095143(38)	−0.096786(35)	−0.096945(17)	−0.089268(70)	−0.090552(71)	−0.090710(31)
d_2 (kHz)	−0.014996(24)	−0.017164(21)	−0.020337(15)	−0.013647(47)	−0.015477(47)	−0.018759(33)
ΔE_0[a] (MHz)	−656707.(539)	0.0	371076.(200)	−589370.(1136)	0.0	320923.(373)
$\sigma_1 G_c$[c] (MHz)	877.8(16)		−484.44(15)	812.4(20)		−454.43(19)
$\sigma_1 G_c^J$ (MHz)	−0.002180(44)		0.0008763(54)	−0.001966(85)		0.0007703(94)
$\sigma_1 G_c^K$ (MHz)	−0.0186(13)		0.01112(22)	[−0.01824][b]		[0.01119][b]
$\sigma_2 W_F$[c] (MHz)	349006.(272)		−204248.(70)	346288.(523)		−201328.(134)
$\sigma_2 W_F^J$ (MHz)	−0.2585(81)		0.2208(24)	−0.309(16)		0.2279(41)
$\sigma_2 W_F^K$ (MHz)	−20.836(51)		12.072(18)	−18.893(81)		11.269(32)
σ_{fit} (MHz)		0.0524[d]			0.0626[d]	
N_{lines}		3542			2185	

[a] Unperturbed vibrational energy difference relative to the energy of the central $\nu_7 2\nu_9$ state.
[b] Assumed value, taken from the $4\nu_9$ triad for $^{35}ClONO_2$.
[c] Only the relative signs of the various Coriolis and Fermi constants can be determined, so that σ_1 and σ_2 can independently be equal to +1 or −1.
[d] Sextic centrifugal distortion constants for the interacting states were fixed at values for the respective ground state, Ref. [16].

Table 4
Spectroscopic constants determined for the $5\nu_9$ triad in $ClONO_2$.

	$^{35}ClONO_2$			$^{37}ClONO_2$		
	$5\nu_9$	$\nu_7 3\nu_9$	$2\nu_7\nu_9$	$5\nu_9$	$\nu_7 3\nu_9$	$2\nu_7\nu_9$
A (MHz)	11624.43(40)	11838.60(22)	12076.13(28)	11622.58(46)	11833.82(41)	12076.46(31)
B (MHz)	2776.739(24)	2770.359(17)	2764.486(11)	2701.266(17)	2694.433(19)	2688.9596(80)
C (MHz)	2279.176(16)	2262.710(13)	2246.651(10)	2228.065(41)	2211.862(26)	2196.517(18)
D_J (kHz)	0.54301(26)	0.52406(19)	0.50630(21)	0.51856(28)	0.50722(45)	0.48402(34)
D_{JK} (kHz)	3.7965(50)	3.9065(79)	3.9679(76)	3.865(24)	3.372(38)	4.027(20)
D_K (kHz)	4.46(12)	5.50(28)	11.41(26)	[4.60][a]	[5.50][b]	[11.41]
d_1 (kHz)	−0.09562(12)	−0.09582(11)	−0.097403(88)	−0.08863(18)	−0.09252(31)	−0.08940(20)
d_2 (kHz)	−0.014153(55)	−0.01681(10)	−0.01891(11)	−0.01318(10)	−0.01477(22)	−0.01770(16)
ΔE_0[c] (MHz)	−767874.(2526)	0.0	489072.(1063)	−679870.(2533)	0.0	448976.(647)
$\sigma_1 G_c$[d] (MHz)	1132.9(19)		-837.7(44)	958.3(61)		−788.4(23)
$\sigma_1 G_c^J$ (MHz)	−0.00155(16)		0.001878(96)	−0.00246(40)		−0.00025(17)
$\sigma_1 G_c^K$ (MHz)	[−0.03][a]		−0.0136(53)	[−0.03][b]		[−0.0136][b]
$\sigma_2 W_F$[d] (MHz)	453754.(1144)		−354131.(440)	462570.(1042)		−351405.(442)
$\sigma_2 W_F^J$ (MHz)	−0.553(27)		0.476(10)	[−0.553][b]		[0.476][b]
$\sigma_2 W_F^K$ (MHz)	−25.38(23)		19.81(16)	−18.76(40)		18.92(16)
σ_{fit} (MHz)		0.0722[e]			0.0806[e]	
N_{lines}		2350			889	

[a] Assumed value, estimated from the averaged progression in ν_9.
[b] Assumed value, taken from the $5\nu_9$ triad for $^{35}ClONO_2$.
[c] Unperturbed vibrational energy difference relative to the energy of the central $\nu_7 3\nu_9$ state.
[d] Only the relative signs of the various Coriolis and Fermi constants can be determined, so that σ_1 and σ_2 can independently be equal to +1 or −1.
[e] Sextic centrifugal distortion constants for the interacting states were fixed at values for the respective ground state, Ref. [16].

The numerical values of the derived effective vibrational separations ΔE are also compared in Table 6. It can be seen that Eq. (5) and (6) allow evaluation of ΔE to considerable precision in spite of the large uncertainties in individual values of ΔE_0 and W_F in Tables 1–4. It is interesting to note that the values of ΔE are very little changed relative to the previous, considerably different fits [13,14], in which this quantity was an explicit parameter of fit. This is not that surprising in view of the fact that the different fitting schemes treat the same data set to comparable accuracy. For the lower dyads interstate transitions have been assigned and those place additional strong constraints on the effective energy separation.

Finally the fitted values of the Fermi resonance parameter for the $(\nu_7 - 1, \nu_9 + 2) \Leftrightarrow (\nu_7, \nu_9)$ interaction can be checked by means of the relation connecting it to the appropriate cubic force constant

$$W_F = \frac{k_{799}}{4\sqrt{2}} \sqrt{\nu_7(\nu_9 + 1)(\nu_9 + 2)}, \tag{7}$$

which was derived in [15] on the basis of treatment given in Ref. [31]. The signs of k_{799} and of W_F are indeterminate from the present results and have been arbitrarily set positive. This relation and associated arguments were used in [15] to estimate W_F and k_{799} on the basis of noted effective nature of the previous rotational constants for the dyads. The values derived in [15] are cited in Table 6 and are compared with the present results. The current fits substantiate previous estimates, and at the same time demonstrate a considerable improvement. The explicitly fitted values of W_F lead to a much tighter spread in the derived values of k_{799} as described by the average $k_{799} = 19.23(13)\ cm^{-1}$ to compare with $k_{799} = 20.5(14)\ cm^{-1}$

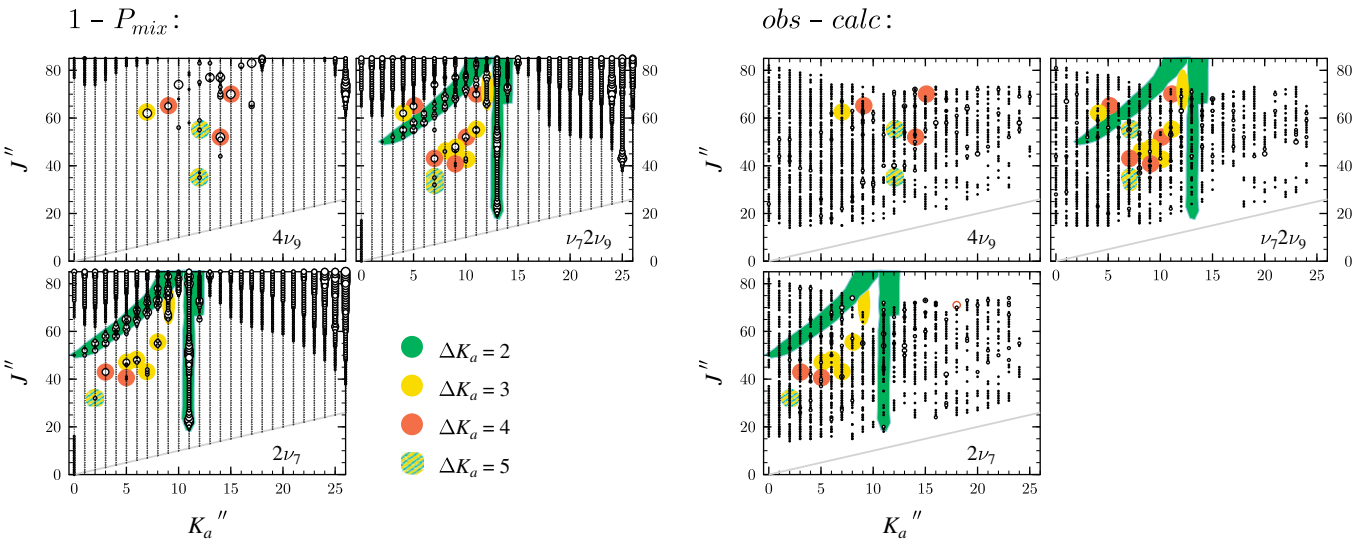

Fig. 5. Data distribution plots for the $4\nu_9$ triad in $^{35}ClONO_2$ as a function of quantum numbers J' and K_a''. The left panes depict the degree of mixing between a given rotational level in one vibrational state with a rotational level in another vibrational state. Black circle diameters are proportional to the value of the quantity $(1 - P_{mix})$, as described in the text. The black circle diameters in the right panes are proportional to absolute values of obs.–calc. differences and those in red are for values exceeding 0.3 MHz. The areas highlighted with background of the same colour are regions of data connected by a given pairwise interstate interaction.

Table 5
Comparison of inertial defects (uÅ^2) for vibrational states in the four lowest $n\nu_9$ polyads in $ClONO_2$.

	$^{35}ClONO_2$			$^{37}ClONO_2$		
	$2\nu_9$	ν_7		$2\nu_9$	ν_7	
Expt.	−1.4443(1)	0.5654(1)		−1.4505(3)	0.5645(3)	
Calc.[a]	−1.4503	0.5668		−1.4564	0.5656	
Expt.–calc.	0.0060	−0.0014		0.0059	−0.0011	
Expt.–calc.[b]	0.2267	−0.2211		0.2663	−0.2579	
	$3\nu_9$	$\nu_7\nu_9$		$3\nu_9$	$\nu_7\nu_9$	
Expt.	−2.2051(3)	−0.2090(3)		−2.2175(5)	−0.2095(5)	
Calc.[a]	−2.2083	−0.1911		−2.2175	−0.1955	
Expt.–calc.	0.0032	−0.0179		0.0000	−0.0140	
Expt.–calc.[c]	0.3546	−0.3668		0.3896	−0.4007	
	$4\nu_9$	$\nu_7 2\nu_9$	$2\nu_7$	$4\nu_9$	$\nu_7 2\nu_9$	$2\nu_7$
Expt.	−2.9698(7)	−0.9808(6)	1.0682(2)	−2.9833(14)	−0.9887(12)	1.0688(3)
Calc.[a]	−2.9662	−0.9491	1.0681	−2.9786	−0.9566	1.0655
Expt.–calc.	−0.0036	−0.0317	0.0001	−0.0047	−0.0321	0.0033
	$5\nu_9$	$\nu_7 3\nu_9$	$2\nu_7\nu_9$	$5\nu_9$	$\nu_7 3\nu_9$	$2\nu_7\nu_9$
Expt.	−3.7425(27)	−1.7615(19)	0.2871(16)	−3.7480(47)	−1.7847(33)	0.2879(22)
Calc.[a]	−3.7242	−1.7070	0.3101	−3.7396	−1.7176	0.3044
Expt.–calc.	−0.0183	−0.0545	−0.0230	−0.0084	−0.0671	−0.0165

[a] Calculated from normal mode inertial defects in Ref. [12] by assuming harmonic-type additivity.
[b] Ref. [13].
[c] Ref. [14].

Table 6
Comparison of the effective energy level differences, Fermi coefficients, and cubic force constants for the $(v_7 - 1, v_9 + 2) \Leftrightarrow (v_7, v_9)$ interactions in the $n\nu_9$ polyads.

$^{35}ClONO_2$							$^{37}ClONO_2$	
	ΔE (MHz)	ΔE/cm^{-1}	W_F (cm^{-1})	k_{799}[a] (cm^{-1})	W_F[b] (cm^{-1})	k_{799}[a,b] (cm^{-1})	ΔE (MHz)	ΔE/cm^{-1}
$2\nu_9 \Leftrightarrow \nu_7$	503804.79(15) 503805.07(79)[c]	16.805119(5) 16.805128(27)[c]	4.842(2)	19.4	5.402(46)	21.6	456438.82(27) 456440.92(138)[c]	15.225160(9) 15.225230(46)[c]
$3\nu_9 \Leftrightarrow \nu_7\nu_9$	729652.45(44) 729650.03(53)[d]	24.338586(15) 24.338506(16)[d]	8.359(4)	19.3	9.570(46)	22.1	682961.3(13) 682976.6(40)[d]	22.781137(43) 22.78165(13)[d]
$4\nu_9 \Leftrightarrow \nu_7 2\nu_9$	858655.46(63)	28.641664(21)	11.641(18)	19.0	12.555(67)	20.5	799671.(13)	26.67415(43)
$5\nu_9 \Leftrightarrow \nu_7 3\nu_9$	1000451.2(70)	33.37146(23)	15.135(38)	19.1			952365.(53)	31.7675(18)
$\nu_7 2\nu_9 \Leftrightarrow 2\nu_7$	436842.02(24)	14.571482(8)	6.813(2)	19.3	6.874(22)	19.5	400932.8(12)	13.373679(40)
$\nu_7 3\nu_9 \Leftrightarrow 2\nu_7\nu_9$	702935.2(96)	23.44740(32)	11.813(15)	19.3	11.531(14)	18.8	664506.(28)	22.1655(9)

[a] Estimated from the fitted value of W_F, see text.
[b] Estimated values from Ref. [15].
[c] Ref. [13].
[d] Ref. [14].

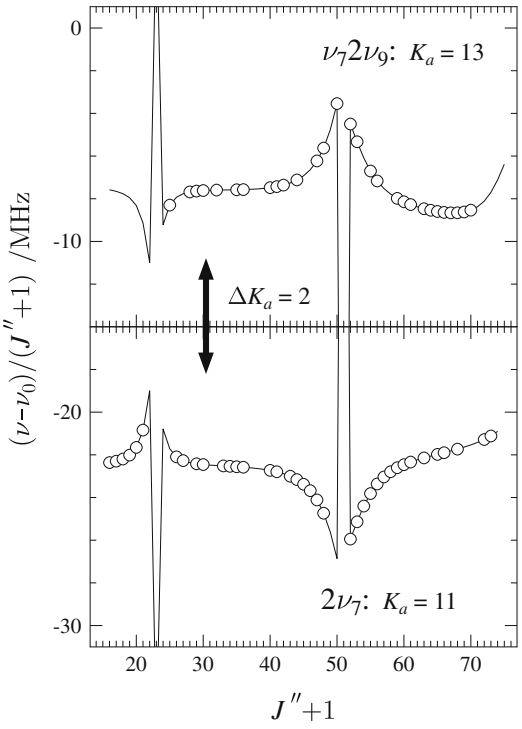

Fig. 6. Frequency difference plots for the main high K_a perturbation sequence between the two upper vibrational states in the $4\nu_9$ triad in $^{35}ClONO_2$ visible in Fig. 5. The two mirror image sequences are for ^{a}R-type transitions between rotational levels with $K_a + K_c = J + 1$.

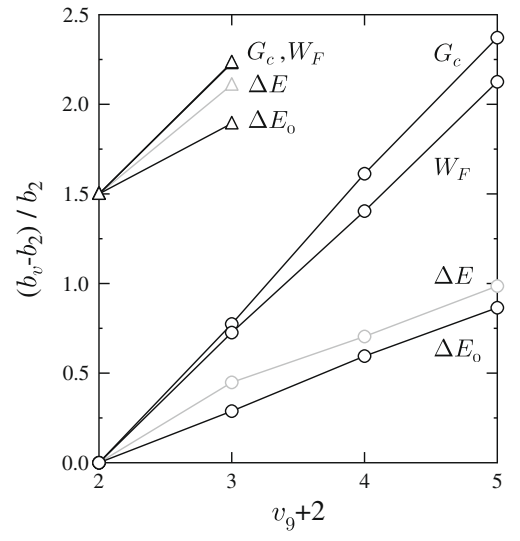

Fig. 7. Plots of scaled changes in energy level differences and in the leading Coriolis and Fermi interaction constants resulting from fitting the $(v_7-1,v_9+2)\Leftrightarrow(v_7,v_9)$ interactions in the nv_9 polyads in $^{35}ClONO_2$. The longer sequence is for $v_7 = 1$, while the shorter sequence is for $v_7 = 2$, and has been shifted upwards by 1.5 for clarity.

based on the estimates from effective behaviour. In this way both the validity of the presently fitted values of W_F and also of the previous interpretation are confirmed. In principle some other cubic constants could also be derived from the values of G_c using Eq. (2) of [30]. The situation is a bit more complex than for W_F and would require some care since a number of cubic constants would be involved, including k_{799}. There is, however, a simplification in that v_9 is an out of plane mode and its inertial derivatives are zero, with the consequence that the harmonic contribution to G_c (the last term in the cited relation) is also zero.

We believe that it is instructive to dwell a bit more on the lessons resulting from comparison of previous [16] and the current fitting schemes for the lowest dyad in $^{35}ClONO_2$ (Table S9). The key differences of the previous Hamiltonian from the current one in Eqs. (1)–(4) are that originally no Fermi terms were employed and that the Coriolis expansion was started at the higher order F_{ab} term instead of G_c. The less efficient performance of the interaction terms was then compensated for by longer centrifugal distortion expansions in the rotational Hamiltonian, reaching up to octic terms. At the same time the centrifugal constants were leading more and in the direction of effective single state fits by taking up perturbation contributions in the form of values approaching the same magnitude but of opposed signs for the participating vibrational states. While this is a reasonably well known phenomenon, there is normally neither the time and/or experience to combat such behaviour, especially if the overall deviation of fit is at an acceptable level. Inspection of changes in centrifugal distortion constants of excited states relative to the values in the ground state is, however, a recommended basic test. In fact the use of all possible assessment criteria of the physical significance of the fitted constants is highly recommended because, once a reasonable fit is obtained for a strongly perturbed situation, it is usually very difficult to change to a radically different fitting model.

The present analysis of the very rich mm-wave rotational spectrum of $ClONO_2$ prepares the ground for assignment of hitherto unassigned states, which are of direct relevance for more accurate recovery of its atmospheric abundance profiles.

Acknowledgements

We like to thank Manfred Winnewisser for the preparation of the $ClONO_2$ sample. Financial support from the Polish Ministry of Science and Higher Education, Grant No. N-N202-0541-33 is gratefully acknowledged. The experimental work at OSU was supported by NASA and the Army Resesarch Office.

Appendix A. Supplementary data

Supplementary data associated with this article are available on ScienceDirect (www.sciencedirect.com) and as part of the Ohio State University Molecular Spectroscopy Archives (http://library.osu.edu/sites/msa/jmsa_hp.htm). Supplementary data associated with this article can be found, in the online version, at doi:10.1016/j.jms.2009.01.005.

References

[1] S. Xu, T.A. Blake, S.W. Sharp, J. Mol. Spectrosc. 175 (1996) 303–314.
[2] A. Goldman, C.P. Rinsland, A. Perrin, J.-M. Flaud, J. Quant. Spectrosc. Radiat. Trans. 60 (1998) 851–861.
[3] J. Ballard, W.B. Johnston, M.R. Gunson, P.T. Wassell, J. Geophys. Res. 93 (1988) 1659–1665.
[4] D.G. Johnson, J. Orphal, G.C. Toon, K.V. Chance, W.A. Traub, K.W. Jucks, G. Guelachvili, M. Morillon-Chapey, Geophys. Res. Lett. 23 (1996) 1745–1748.
[5] J.L. Domenech, J.-M. Flaud, G.T. Fraser, A.M. Andrews, W.J. Lafferty, P.L. Watson, J. Mol. Spectrosc. 183 (1997) 228–233.
[6] J.-M. Flaud, J. Orphal, W.J. Lafferty, M. Birk, G. Wagner, J. Geophys. Res. Atmos. 107 (2002) 4782.
[7] D.T. Petkie, T.M. Goyette, P. Helminger, H.M. Pickett, F.C. De Lucia, J. Mol. Spectrosc. 208 (2001) 121–135.
[8] D.T. Petkie, P. Helminger, B.P. Winnewisser, M. Winnewisser, R.A.H. Butler, K.W. Jucks, F.C. De Lucia, J. Quant. Spectrosc. Rad. Trans. 92 (2005) 129–141.
[9] R.A.H. Butler, PhD Dissertation, The Ohio State University, Columbus, 2002.
[10] R.D. Suenram, D.R. Johnson, J. Mol. Spectrosc. 65 (1977) 239–248.
[11] R.D. Suenram, F.J. Lovas, J. Mol. Spectrosc. 105 (1984) 351–359.
[12] H.S.P. Müller, P. Helminger, S.H. Young, J. Mol. Spectrosc. 181 (1997) 363–378.
[13] R.A.H. Butler, S. Albert, D.T. Petkie, P. Helminger, F.C. De Lucia, J. Mol. Spectrosc. 213 (2002) 8–14.
[14] R.A.H. Butler, D.T. Petkie, P. Helminger, F.C. De Lucia, J. Mol. Spectrosc. 220 (2003) 150–152.

[15] D.T. Petkie, R.A.H. Butler, P. Helminger, F.C. De Lucia, J. Mol. Struct. 695–696 (2004) 287–293.
[16] R.A.H. Butler, D.T. Petkie, P. Helminger, F.C. De Lucia, Z. Kisiel, J. Mol. Spectrosc. 243 (2007) 1–9.
[17] R.A.H. Butler, D.T. Petkie, P. Helminger, F.C. De Lucia, E. Białkowska-Jaworska, Z. Kisiel, J. Mol. Spectrosc. 244 (2007) 113–116.
[18] D.T. Petkie, T.M. Goyette, R.P.A. Bettens, S.P. Belov, S. Albert, P. Helminger, F.C. De Lucia, Rev. Sci. Instrum. 68 (1997) 1675–1683.
[19] I. Medvedev, M. Winnewisser, F.C. De Lucia, E. Herbst, E. Białkowska-Jaworska, L. Pszczółkowski, Z. Kisiel, J. Mol. Spectrosc. 228 (2004) 314–328.
[20] P. Groner, M. Winnewisser, I.R. Medvedev, F.C. De Lucia, E. Herbst, K.V.L.N. Sastry, Astrophys. J. Suppl. Ser. 169 (2007) 28–36.
[21] Z. Kisiel, L. Pszczółkowski, I.R. Medvedev, M. Winnewisser, F.C. De Lucia, E. Herbst, J. Mol. Spectrosc. 233 (2005) 231–243.
[22] Z. Kisiel, PROSPE – Programs for ROtational SPEctroscopy, Available from: <http://info.ifpan.edu.pl/~kisiel/prospe.htm>.
[23] Z. Kisiel, O. Dorosh, M. Winnewisser, M. Behnke, I.R. Medvedev, F.C. De Lucia, J. Mol. Spectrosc. 246 (2007) 39–56.
[24] H.M. Pickett, J. Mol. Spectrosc. 148 (1991) 371–377.
[25] H.M. Pickett, SPFIT/SPCAT package, Available from: <http://spec.jpl.nasa.gov>.
[26] H.A. Jahn, Phys. Rev. 56 (1939) 680–683.
[27] J.K.G. Watson, in: J.R. Durig (Ed.), Vibrational Spectra and Structure, vol. 6, Elsevier, New York/Amsterdam, 1977, pp. 1–89.
[28] D. Papoušek, M.R. Aliev, Molecular Vibrational/Rotational Spectra, Academia, Prague, 1982, Section 17.8.
[29] A.R. Hoy, J. Mol. Spectrosc. 86 (1981) 55–64.
[30] C.D. Esposti, F. Tamassia, G. Cazzoli, Z. Kisiel, J. Mol. Spectrosc. 170 (1995) 582–600.
[31] C.H. Townes, A.L. Schawlow, Microwave Spectroscopy, McGraw-Hill, New York, 1955.